ADVANCED FUNCTIONAL MATERIALS
www.afm-journal.de

Ionic Liquid-Based Reversible Metal Electrodeposition for Adaptive Radiative Thermoregulation Under Extreme Environments

Jiawei Liang, Chenxi Sui, Jiacheng Tian, Genesis Higueros, Ting-Hsuan Chen, Ronghui Wu, Pei-Jan Hung, Yang Deng, Natalie Rozman, Willie John Padilla, and Po-Chun Hsu**

This paper presents the development of an electrochemically-driven variable emission thermoregulating device designed for efficient radiative heat management across various temperature environments. Utilizing the ionic liquid 1-butyl-3-methylimidazolium tetrafluoroborate ($BMIMBF_4$), the study explores its thermal and electrochemical stability, low vapor pressure, and excellent performance over a wide operational temperature range, making it an ideal electrolyte. The device uses mid-infrared electrochromic technology, employing ultra-wideband transparent conductive electrodes and reversible metal electrodeposition to dynamically adjust thermal emissivity between 0.06 and 0.89. This capability allows for significant improvements in heat management, offering a responsive and adaptable solution compared to current systems. The findings suggest that such advanced materials and mechanisms can enhance energy management in spacecraft, potentially extending to other space fields requiring precise thermal control.

1. Introduction

As the global population grows and energy demand continues to rise, effective mitigation of energy consumption becomes an increasingly urgent need.[1] Buildings and infrastructure account for ≈40% of global energy use,[2] and thermoregulation constitutes a majority of this usage. However, problems such as inefficient thermal management in these infrastructures result in a significant waste of energy. Research suggests that two-thirds of the world's energy is dissipated in the form of heat.[3] This energy loss is primarily due to outdated heating, ventilation, and air conditioning (HVAC) systems, and poor building insulation,[4] which is not only wasteful but also exacerbates environmental issues.

To solve these problems, we can resort to radiative heat transfer and use the characteristics of mid-infrared radiation (mid-IR) to improve thermal management. Mid-infrared radiation, with wavelengths ranging from 3 to 50 microns, aligns closely with the thermal radiation wavelengths emitted by most objects in our environment,[5] making it ideal for thermoregulation. In particular, in the "atmospheric window" regime of 8 to 14 microns, the absorption is minimal, allowing terrestrial thermal radiation to freely transmit into deep space.[6] New materials have been developed to take advantage of the atmospheric window, which can be incorporated with other multispectral engineering for maximizing heating/cooling performances. Among them, electrochromic materials are a particularly promising type, as they can dynamically modulate optical properties in response to an electrical signal, thereby controlling the amount of energy absorbed or emitted, which is essential for adapting to the ever-changing environment and heating/cooling demands.[7–11] Recent advancements in electrochromic technology have resulted in new materials and devices with improved performance and durability.[12–16]

This study presents an electrochemically-driven variable emission thermoregulating technology, demonstrating its ability to regulate temperature by modulating the mid-IR radiation in response to electrical output. We successfully prove that our technology can achieve emissivity(ϵ) tuning between 0.06 and 0.89 ($\Delta\epsilon = 0.83$), which has the potential for smart and adaptive building envelopes that can reduce the HVAC energy consumption.

J. Liang, J. Tian
University Program in Materials Science and Engineering
Duke University
Durham, NC 27708, USA

C. Sui, G. Higueros, T.-H. Chen, R. Wu, P.-J. Hung, P.-C. Hsu
Pritzker School of Molecular Engineering
University of Chicago
Chicago, IL 60637, USA
E-mail: pochunhsu@uchicago.edu

T.-H. Chen, Y. Deng, N. Rozman, W. J. Padilla
Department of Electrical and Computer Engineering
Duke University
Durham, NC 27708, USA
E-mail: willie.padilla@duke.edu

G. Higueros
Thomas Department of Mechanical Engineering and Materials Science
Duke University
Durham, NC 27708, USA

The ORCID identification number(s) for the author(s) of this article can be found under https://doi.org/10.1002/adfm.202419087

DOI: 10.1002/adfm.202419087

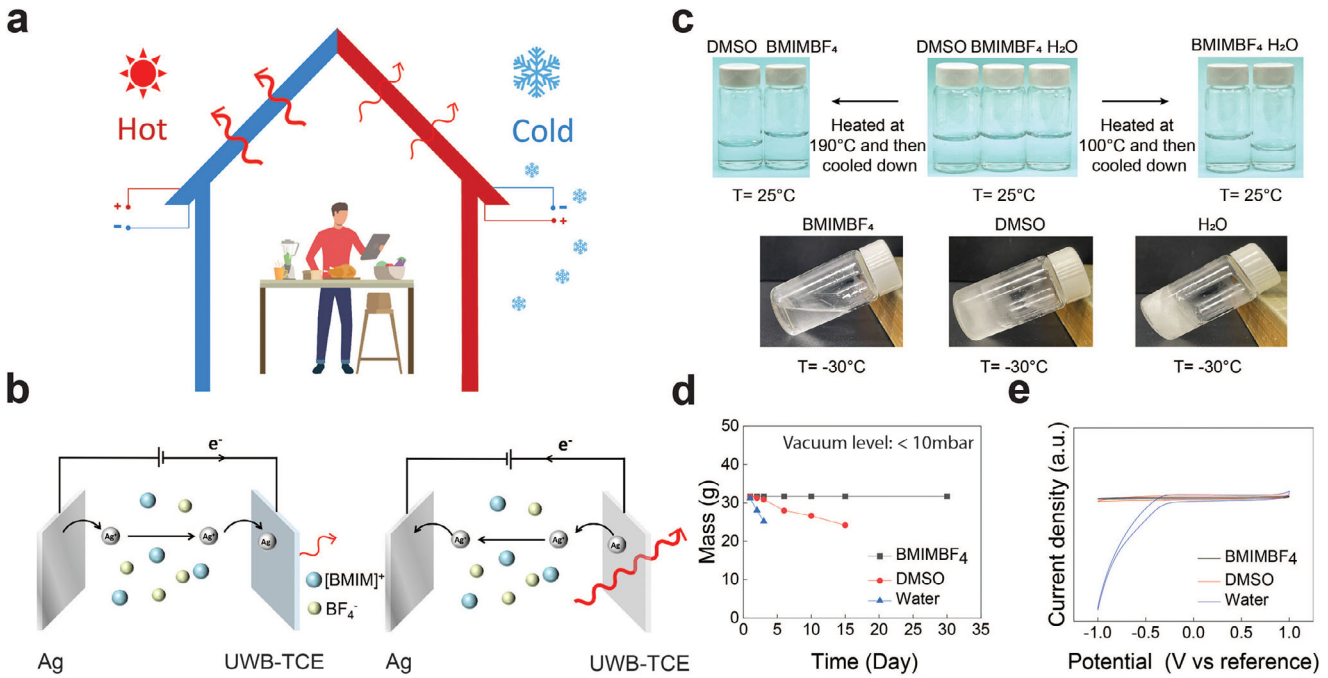

Figure 1. Concept and advantages of electrochromic mid-IR modulation system with an ionic liquid electrolyte. a) Visual concept of radiative thermoregulation b) Graphic demonstration of the electrochromic system. The whole technology can be electrochemically tuned between the heating mode (Ag-deposited) and the cooling mode (Ag-stripped). UWB-TCE stands for ultra-wideband transparent conducting electrode. c) Thermal stability test of ionic liquid 1-Butyl-3-methylimidazolium tetrafluoroborate ($BMIMBF_4$), DMSO, and Water. Only $BMIMBF_4$ remains unchanged at these extreme temperatures. d) Mass change of $BMIMBF_4$, DMSO, and water in vacuum at 25 °C. e) Cyclic voltammograms on ITO with $BMIMBF_4$, water, and DMSO. The experiments were conducted at room temperature and the reference electrodes of water, DMSO, and $BMIMBF_4$ are commercial Ag/AgCl (saturated KCl solution) electrode, Ag/Ag^+ (0.01 M $AgNO_3$ in DMSO) electrode, and Pt wire, respectively. The scanning rate is 50 mV s^{-1}.

In addition, we employed an ionic liquid as the solvent, enabling efficient and reliable performance over a wide temperature range due to its low volatility and high thermal stability. Thermal capability is crucial in building applications where extreme temperature conditions are common, from the freezing cold of winter to the sweltering heat of summer. In more extreme cases, such as spacecraft applications, ionic liquid robustness is indispensable.

2. Device Structure

Figure 1a illustrates how the thermoregulating electrochemically-driven variable emission device (Thermo-EVED) enables the building to manage thermal stability by applying an electrical bias. The mid-IR electrochromic apparatus, as depicted in Figure 1b, consists of the ultra-wideband transparent conductive electrode (UWB-TCE), a silver foil as the counter electrode, and the $AgBF_4$, $BMIMBF_4$ solution as the electrolyte. The UWB-TCE is a Pt-modified monolayer graphene with gold microgrids, where the structure is optimized to achieve high mid-IR transmissivity and both short- and long-range electrical conductivity.[11,17] The high transmissivity of the UWB-TCE allows the underlying high IR-absorbing electrolyte (Figure S1, Supporting Information) to exhibit high emissivity at the stripped (no metal) state, which corresponds to the cooling state with enhanced radiative heat exchange. Here, we apply Kirchhoff's Law, which asserts that, at thermodynamic equilibrium, emissivity must equal absorptivity ($\epsilon = \alpha$).[18] As the silver gradually deposits onto the transparent electrode, the Ag nanoparticles electroplate on the Pt-modified graphene, creating a thicker and denser metal layer, which increases the IR reflectivity and contributes to the low-ϵ heating state, reducing the radiative heat loss.

3. Ionic Liquid Electrolyte System

To enable the technology to function properly across a wide range of temperatures, the electrolyte must possess excellent thermal stability. Compared to conventional electrolytes like DMSO and water, ionic liquids have gained considerable attention as a sustainable class of green solvents due to their unique physicochemical properties. Among ionic liquids, $BMIMBF_4$ exhibits good properties on i) thermal stability,[19–21] ii) electrochemical stability,[22,23] and iii) low vapor pressure,[19,21,24] which makes it a versatile solvent for a broad range of applications. $BMIMBF_4$ can operate across a wide temperature range, maintaining durability from −71 °C to 300 °C.[25] We performed an experiment by heating the same volume of $BMIMBF_4$, water, and DMSO to 190, 100, and 190 °C, respectively, for 20 min and then cooled to 25 °C. The results show that $BMIMBF_4$ underwent minimal changes after the heating test, demonstrating its notable thermal stability, while DMSO and water both had significant evaporative mass loss (Figure 1c). At low temperatures of −30 °C, $BMIMBF_4$ maintained its liquid state, which was essential for fast ion transport; however, water and DMSO freeze at these temperatures. Moreover, the low vapor pressure of $BMIMBF_4$ is another

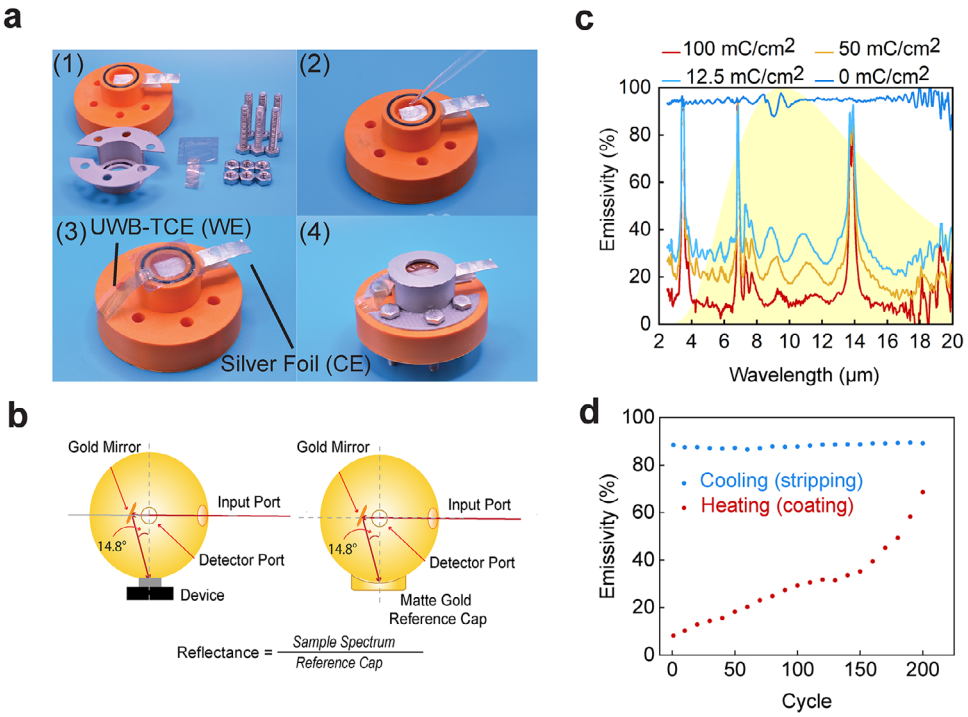

Figure 2. Device for measuring the emissivity and results. a) The Thermo-EVED for emissivity measurement. (1)–(4) are the assembling procedures. b) The configuration of measuring reflectivity with a diffuse gold integrating sphere in Fourier-transform infrared spectroscopy (FTIR). c) Emissivity spectra as the function of electrodeposited charge capacity. d) Weighted-average emissivity at cooling and heating states versus switching cycles.

important property that minimizes solvent loss due to evaporation and ensures the permanence of the electrolyte over an extended period.[26] It can also be a key merit for space applications. As shown in Figure 1d, the same amount of DMSO, water, and $BMIMBF_4$ were placed into a vacuum chamber at the temperature of 26 °C, and their masses were recorded every day. It is observed that both DMSO and water had decreased in weight, whereas $BMIMBF_4$ maintained its original mass for an extended duration. Figure 1e further compares the electrochemical stability of $BMIMBF_4$ with water and DMSO. The plot demonstrates that both $BMIMBF_4$ and DMSO exhibit minimal electrochemical current density from −1 to 1 V versus Ag and Pt wire, respectively, showing good electrochemical permanence In contrast, water has the hydrogen evolution reaction (HER), contributing to the downward slope at the cathodic potential.[27] Overall, the unique physicochemical properties of $BMIMBF_4$ make it an excellent solvent for various applications, particularly those requiring thermal, vacuum, and electrochemical stability.

4. Method of Measuring Emissivity and Results

We further investigated the instrument's emissivity tuning performance. We first designed and 3D printed an apparatus for sealing the electrochemical cell. The 3D printing material is polylactic acid. The apparatus consists of upper and lower parts with O-rings and screws, as shown in **Figure 2**a. The entire assembly process is conducted inside a glove box filled with argon, where the moisture and oxygen content is kept below 1 ppm. The inclusion of an O-ring seals the entire device, minimizing the atmospheric influence when the Thermo-EVED is measured outside the glove box. The electrochemical cell is a two-electrode system, with silver foil as the counter electrode. The silver foil is affixed by using epoxy, ensuring a stable connection. The electrolyte is carefully filled into the cell, followed by the working electrode placed on the top. The cell holder and upper casing are then combined and screwed together. We then use cyclic voltammetry (CV) to identify water and oxygen in the system. The CV plot under water- and oxygen-free conditions is shown in **Figure 3**a, and the CV curve in the atmospheric environment is shown in Figure S2 (Supporting Information) for comparison. We measured the reflectivity and used Kirchhoff's law to calculate the emissivity (Figure 2b). The details are in the Supporting Information.

Figure 2c illustrates how the electrodeposited charge capacity affects the emissivity of the Thermo-EVED. As the cathodic current flows to the working electrode, silver ions are reduced, which results in a silver film on the electrode,[28,29] leading to an increase in its reflectivity and therefore a decrease in emissivity. Notably, the electrochromic system can operate at various emissivity levels, providing continuous and delicate radiative thermoregulation. Figure 2c demonstrates that the Thermo-EVED 's wavelength average emissivity can be maintained at levels of 0.9, 0.35, and 0.1 by adjusting the electrodeposited charge capacity to 0 (blue curve), 12.5 (light blue), and 100 (red) mC cm^{-2}, respectively.

During the electroplating process, the silver particles deposited on the working electrode are initially sparse and discrete. As more silver is reduced and electrodeposited, the silver nuclei begin to reach the percolation threshold,[30] the individual particles merge into an interconnected metallic mesh,

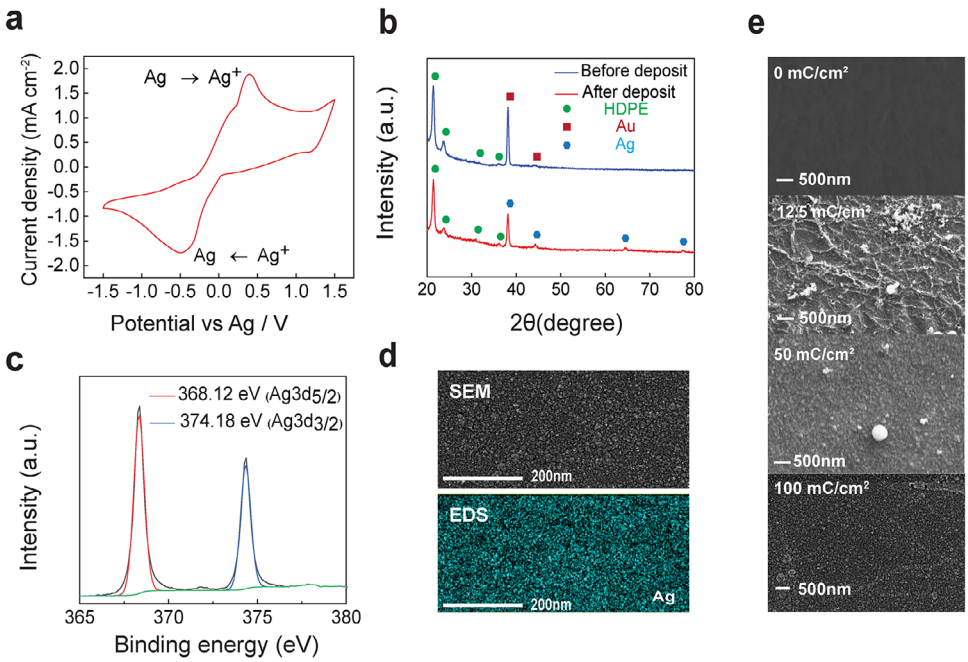

Figure 3. Emissivity tuning mechanism and characterization analysis. a) Cyclic voltammogram of $BMIMBF_4$ electrolyte using Ag as a pseudo-reference electrode. The scan rate is 50 mV s^{-1} with a silver foil as the counter electrode and UWB-TCE as the working electrode. b) XRD and c) XPS analysis of the electrodeposited film. d) SEM image and EDS mapping of the deposited Ag film. e) SEM image at different charge capacities.

resulting in a sudden drop in emissivity. This explains why a decrease in emissivity is observed when the charge density reaches 12.5 mC cm^{-2}. However, as the electroplating continues and the silver layer becomes thicker, the emissivity stabilizes and changes little. Therefore, between charge densities of 12.5 to 50 mC cm^{-2}, there is still a decrease in emissivity, but it is relatively small.

We further tested the cycle life of the Thermo-EVED, as shown in Figure 2d. The emissivity contrast began at more than 80% and degraded to ≈60% after 100 cycles. It is important to note that the heating state (low-ϵ) degrades more rapidly than the cooling state (high-ϵ). This could be due to the corrosive effect of bromide ions on the gold grid, causing it to break and increase the resistance of the working electrode over time, as shown in Figure S3 (Supporting Information).[31] As a result, the silver deposition process becomes more challenging, and the silver film on the working electrode becomes less dense, leading to a decrease in emissivity. To assess the long-term stability of the deposited silver layer in the heating state, we performed extended cycling tests and monitored the emissivity evolution over 350 cycles, as shown in Figure S4 (Supporting Information). To enhance electrode durability and mitigate bromide-induced corrosion, we increased the gold microgrid thickness from 200 to 600 nm and applied a 6 nm Pt coating to the surface. The thicker gold layer provides greater structural stability, while the Pt coating enhances corrosion resistance. Despite these improvements, emissivity in the heating state gradually increases over time. In contrast, the cooling state remains stable, indicating effective stripping. On the other hand, the emissivity of the cooling state remains relatively unchanged since bromide ions can corrode silver,[31] and any remaining silver on the electrode can be corroded by the bromide in the electrolyte.

5. Elemental Characterization and Mid-IR Tunability Analysis

Cyclic voltammetry (CV) is used to analyze the reaction during electrodeposition to further investigate the emissivity tuning mechanism. Scanning electron microscope (SEM), X-ray photoelectron spectroscopy (XPS), X-ray diffraction (XRD), and energy-dispersive X-ray spectroscopy (EDS) are used to characterize the surface morphology and elemental composition of the electrodeposited metal film. The electrochemical properties of the electrolyte, which comprises the ionic liquid $BMIMBF_4$, $AgBF_4$, and tetrabutylammonium bromide (TBAB), were investigated inside a glove box. Three-electrode CV was implemented to investigate the electrochemical potentials of metal deposition and dissolution. UWB-TCE was used as the working electrode, Ag foil was employed as the counter electrode, and silver wire was used as the reference electrode. As depicted in Figure 3a, the ionic liquid displays an electrochemical window of at least 3 V, ranging from −1.5 to +1.5 V versus Ag reference. The anodic current increase at a potential of ≈−0.1 V is attributed to the oxidation of the silver present on the working electrode, while the cathodic current decrease at a potential of ≈0 V corresponds to the reduction of the silver. The electrochemical redox reaction mechanisms for the electrodeposition and dealloying of Ag ions in the electrolyte proceeded as follows:

Ag reduction reaction:

$$AgBr_n^{1-n} + e^- \rightarrow Ag + nBr^- \quad (1)$$

Oxidation of the Ag:

$$Ag \rightarrow Ag^+ + e^- \quad (2)$$

$$Ag^{+} + nBr^{-} \rightarrow AgBr_{n}^{1-n} \quad (3)$$

The formation and dissolution of the silver mirror can be explained by the electrochemical reduction and oxidation processes of Ag ions in the electrolyte solution. When Ag^{+} complex ions (AgX_{n}^{1-n}) are electrochemically reduced to silver, forming a bright mirror film with low emissivity.[32] This film then undergoes oxidation when the voltage polarity is reversed. The presence of Br^{-} in the electrolyte solution is essential for mediating the oxidative deposition of Ag since the oxidation potentials associated with $3Br^{-}$ to Br^{3-}, which is 1.5 V,[32] are higher than that of electroplated metal Ag to Ag^{+}. This allows the deposited Ag to be fully oxidized to Ag^{+} through the mediation of Br^{-}, increasing spectral transmittance. We compared two different electrolytes and showed the images in Figure S5 (Supporting Information).

The composition of the electrodeposited metal film was characterized by X-ray photoelectron spectroscopy (XPS) and X-ray diffraction (XRD). XRD analysis reveals peaks at 38.19°, 46.18°, 67.44°, and 77.70° on the ultra-wideband transparent electrode, which can be assigned to Ag (111), Ag (200), Ag (220), and Ag (311),[33] as shown in Figure 3b. In Figure 3c, the peaks at 368.12 and 374.18 eV in the Ag 3d scan confirm the existence of the metallic Ag (0).[34] Figure 3d shows the morphology and elemental mapping by SEM and EDS, indicating dense and uniform silver plating. Figure 3e shows the temporal evolution of the working electrode surface as the charge capacity increases. It can be seen that as the charge capacity elevates, the silver particles on the UWB-TCE surface become larger and denser. The SEM images also effectively illustrate the impact of temperature on silver electrodeposition, as shown in Figure S6 (Supporting Information). At −2 °C, the deposition results in large, sparsely distributed silver particles, indicating slow nucleation and growth due to reduced ion mobility. At room temperature, a more uniform and densely packed distribution of smaller particles is observed, suggesting an optimal balance between nucleation and growth. In contrast, high-temperature electrodeposition leads to a significantly increased particle density with smaller, interconnected clusters, highlighting an enhanced nucleation rate and rapid deposition kinetics. These findings visually demonstrate how temperature influences the morphology and distribution of silver particles, making it a crucial factor in controlling electrodeposition outcomes.

6. Electrochromic Device Performance at Different Temperatures and Mechanical Properties

The unique property of ionic liquid allows us to further study its capability to operate within a wide temperature range. **Figure** 4a shows the life cycle test of the Thermo-EVED in different ambient conditions. The initial state of the Thermo-EVED exhibited equivalent emissivity in both the heating and cooling states at 75, 25, and −2 °C. After 100 cycles, the emissivity of the heating state at 75 °C remains the lowest among the three working temperatures. During the low-temperature test, it was observed that the electroplating process became much more difficult due to the low conductivity of the electrolyte, as shown in Figure 4b. As a result, at the 100th cycle of the cycle life test, the low current flow impeded the electrodeposition process, and a dense silver film could not be adequately formed, leading to a higher emissivity compared to the ambient temperature conditions.

To experimentally demonstrate our technology's thermoregulation capability, we perform thermal imaging on our variable emittance prototype and other control samples at various temperatures. Electroplating was employed to adjust the emissivity, as depicted in Figure 4c. Three distinct sets of material parameters were tested: high-ϵ material, low-ϵ material, and our Thermo-EVED with tunable emissivity. Throughout the experiments, we controlled the deposition process to maintain the IR-apparent temperature at 38 °C. As the actual hot plate temperature increased, we observed a gradual rise in temperature for both the high-ϵ and low-ϵ states. Notably, in the modulated-ϵ state, the temperature indeed remained constant, as illustrated in Figure 4d. These results demonstrate the device's capability to regulate the material's reflectance to maintain the radiative heat flux, thereby stabilizing the system heat balance. By effectively modulating the emissivity, our technology offers potential applications in thermal management and control systems. Finally, as shown in Figure 4e the material choice combination provides UWB-TCE with mechanical flexibility. The sheet resistance remained stable during 500 bending cycles at the radius of 0.67 cm as shown in Figure 4f. Such bending performance is beneficial for conformal bonding with minimal thermal interface resistance. A bending test was conducted on the electrochromic device, as shown in Figure 4g, demonstrating its structural integrity at a bending radius of 0.4 cm and confirming its mechanical flexibility. Infrared thermal imaging shown in Figure 4h further reveals that the device maintains its cooling and heating states even when deformed.

7. Outlook and Future Prospects

Based on the unique properties of the ionic liquid electrolyte, our device offers promising applications for space stations where proper temperature management is critical. The temperature in outer space exhibits dramatic fluctuations, influenced heavily by location and exposure to sunlight.[35–37] Thus, thermal control is an important aspect of spacecraft design. However, current thermal control systems on the space station have limitations in their ability to respond quickly to changing temperature conditions. They also have problems such as significant power consumption and heavy weight.[38,39]

There are three fundamental heat transfer mechanisms: conduction, convection, and radiation.[40] Because space is essentially a vacuum, lacking a medium for conduction and convection, radiation becomes the only heat transfer method. Our study introduces an electrochemically-driven variable emission thermoregulating prototype that operates effectively across a broad temperature range. This technology can adjust its emissivity from 0.06 to 0.89 ($\Delta\epsilon = 0.83$), showing significant promise for integration into spacecraft thermal control systems, as shown in **Figure** 5. It offers marked improvements in responsiveness and adaptability over existing methods, which could be used in the spacecraft.

This research uses $BMIMBF_4$, an ionic liquid electrolyte, to demonstrate a radiative thermoregulator for extreme conditions. The exceptional thermal stability, electrochemical stability, and

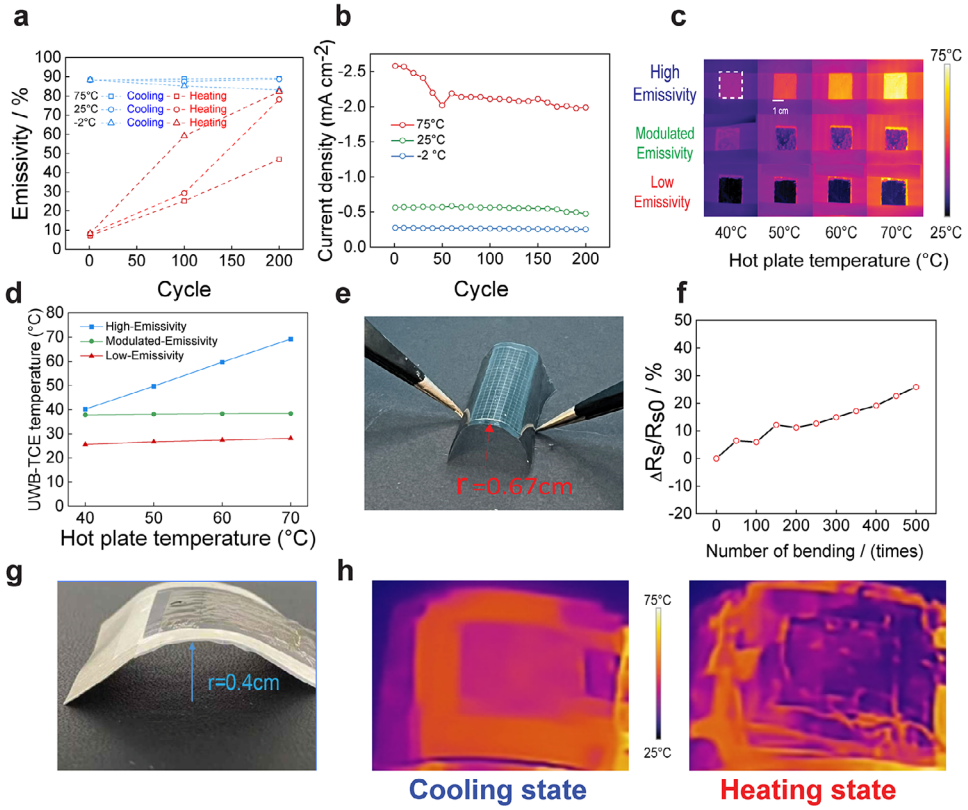

Figure 4. Device test on different temperatures and mechanical properties. a) Weighted-average emissivity at cooling and heating states versus cycles at 75, 25, and −2 °C. b) The current density in the cycle life test at 75, 25, and −2°C, which illustrates the positive correlation between electrochemical activity and temperature. c) Thermal images of the electrochromic devices at different emissivities and hot plate temperatures. Note the modulated emissivity means the Thermo-EVED is actively controlled to stabilize the radiative heat loss. d) The average apparent temperatures measured by the thermal camera. e) Picture of the bending test configuration. f) Cyclic bending test with a bending radius of 0.67 cm. g) Picture of the bending test of the device. h) Thermal images of the electrochromic device at bending conditions.

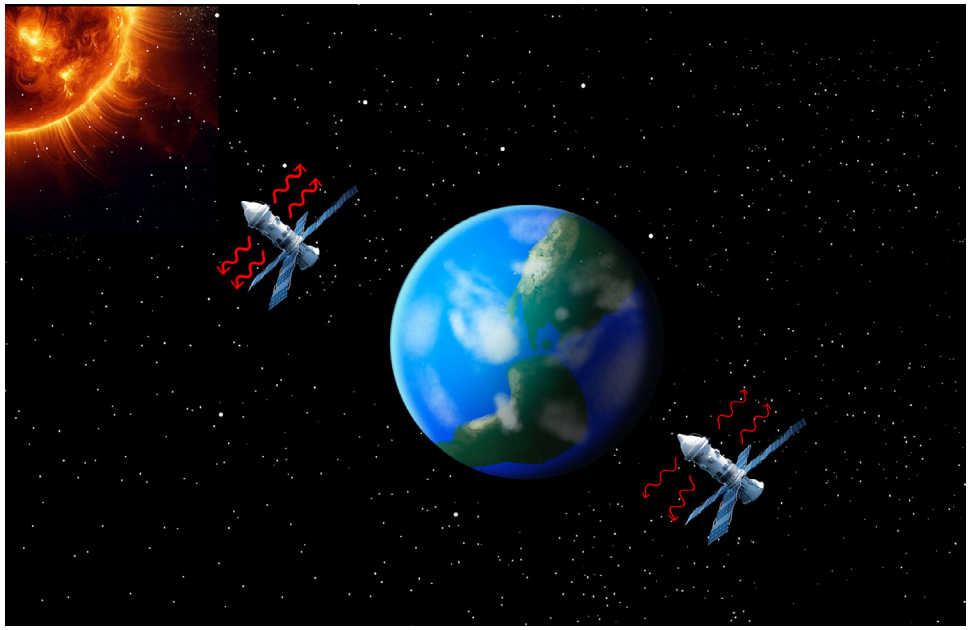

Figure 5. Conceptual schematics of radiative thermoregulation in space.

low vapor pressure of $BMIMBF_4$ make it well-suited for these applications. During the electroplating process, the tunability of Ag deposition is demonstrated, showcasing a thermal emissivity contrast of 0.83 and long-term durability. Furthermore, the morphology of the electrodeposited metal on the electrode is characterized using XRD, SEM, and XPS analysis. The study demonstrates the performance of the electrochromic technology at temperatures ranging from −2 to 75 °C while maintaining a thermal emissivity contrast of 0.83. By varying the emissivity, the radiative heat flux can be maintained, thereby stabilizing the thermal environment of the device in interest. These findings have implications for the design of probes and instruments intended for outer space applications and contribute to a deeper understanding of metal electrodeposition in ionic liquid electrolytes.

8. Experimental Section

Chemicals: 1-Butyl-3-methylimidazolium tetrafluoroborate ($BMIMBF_4$), silver tetrafluoroborate ($AgBF_4$), tetrabutylammonium bromide (TBA-Br) were purchased from Aldrich and used without further purification. The silver wire and silver film were obtained from BASi company.

Synthesis of Electrodes: To synthesize the optical thin film, the photoresist was spin-coated on graphene-copper foil for 3000 RPM in 30 s and grown on the silicon plate. After spinning, the sample was baked at 90 °C for 1 min on a hotplate. The sample was put into the MA6 Mask Aligner and exposed to UV light for 13.5 s. Then, the sample was washed and heated at 90 °C for 2 min in the oven. E-beam & Thermal Metal Evaporator (Kurt Lesker PVD 75) was used for evaporating Au and Cr with thicknesses of 20 and 2 nm, respectively. Finally, graphene was transferred from the copper foil to PE film through a hot press machine, and the copper was eroded by iron (III) chloride.

Preparation of Electrolytes: The electrolyte was prepared by stirring 1-Butyl-3-methylimidazolium tetrafluoroborate (10.0 mL) with silver tetrafluoroborate (50.0 мм) at 25 °C for 3 h. Tetrabutylammonium bromide (TBA-Br) (60.0 mmol) was then added to the mixture and the stirring continued for 4 h at 65 °C.

Electrochemistry: The electrochromic performance tests were conducted via VMP3 (BioLogic Inc.). For the constant potential electrodeposition process, the potential was −0.5 V (vs Ag wire) for the 3-electrode system. For the constant potential stripping process, the potential was +0.5 V for the 3-electrode cell (vs Ag wire). The cyclic voltammetry test was scanned at a rate of 50 mV s^{-1}.

Characterization: Fourier transform infrared (FT-IR) spectra were obtained on a Specode 75 model spectrometer in the range of 400−4000 cm^{-1}. The morphology of Ag nanoparticles on the electrode was observed by a scanning electron microscope (Apreo S by ThermoFisher Scientific). The current−voltage measurements were performed on Autolab PGSTAT 302N electrochemical workstation.

Supporting Information

Supporting Information is available from the Wiley Online Library or from the author.

Acknowledgements

The authors thank the Shared Materials Instrumentation Facility at Duke University for assisting the equipment use. P.C.H. acknowledges the financial support from the National Science Foundation (ECCS Award No. 2324286).

Conflict of Interest

The authors declare no conflict of interest.

Author Contributions

P.C.H. and J.L. conceived the idea. J.L. performed all the experiments, conducted optical fitting, simulated the device design, and analyzed their corresponding data. T.C., N.R., Y.D., and W.J.P. helped with the emissivity measurement. J.T. and R.W. recorded the thermal images. C.S., P.H., and G.H. helped with the transparent electrode fabrication. J.L. and P.C.H. wrote the manuscript with input from all co-authors.

Data Availability Statement

The data that support the findings of this study are available from the corresponding author upon reasonable request.

Keywords

electrochemically-driven, mid-infrared electrochromic, thermal emissivity, thermoregulating device, variable environment

Received: October 9, 2024
Revised: February 25, 2025
Published online: April 24, 2025

[1] a) M. Santamouris, K. Vasilakopoulou, *e-Prime-Adv. Electrical Eng., Electron. Energy* **2021**, *1*, 100002; b) Z. Wang, T. Hong, *Appl. Energy* **2020**, *269*, 115036; c) W. Strielkowski, I. Firsova, I. Lukashenko, J. Raudeliūnienė, M. Tvaronavičienė, *Energies* **2021**, *14*, 893.
[2] a) M. González-Torres, L. Pérez-Lombard, J. F. Coronel, I. R. Maestre, D. Yan, *Energy Reports* **2022**, *8*, 626; b) A. M. Omer, *Renew. Sustain. Energy Rev.* **2008**, *12*, 2265.
[3] a) A. Firth, B. Zhang, A. Yang, *Appl. Energy* **2019**, *235*, 1314; b) L. Miró, J. Gasia, L. F. Cabeza, *Appl. Energy* **2016**, *179*, 284.
[4] a) R. Aridi, J. Faraj, S. Ali, M. Gad El-Rab, T. Lemenand, M. Khaled, *Energies* **2021**, *14*, 5869; b) M. Ortiz, L. Itard, P. M. Bluyssen, *Energy Build.* **2020**, *221*, 110102.
[5] a) D. Jung, S. Bank, M. L. Lee, D. Wasserman, *J. Opt.* **2017**, *19*, 123001; b) H. Kaplan, *Practical Applications of Infrared Thermal Sensing and Imaging Equipment*, SPIE Press, Bellingham, WA, **2007**, *75*.
[6] a) H. Harde, *Int. J. Atmospheric Sciences* **2013**, *2013*, 503727; b) R. Sun, P. Zhou, W. Ai, Y. Liu, Y. Li, R. Jiang, W. Li, X. Weng, L. Bi, L. Deng, *Opt. Express* **2019**, *27*, 11537; c) H. Zhu, Q. Li, C. Tao, Y. Hong, Z. Xu, W. Shen, S. Kaur, P. Ghosh, M. Qiu, *Nat. Commun.* **2021**, *12*, 1805; d) M. Wei, W. Wu, D. Li, H. Xu, Y. Lu, W. Song, *Sol. Energy* **2020**, *207*, 471.
[7] A. Llordés, G. Garcia, J. Gazquez, D. J. Milliron, *Nature* **2013**, *500*, 323.
[8] A. L.-S. Eh, M.-F. Lin, M. Cui, G. Cai, P. S. Lee, *J. Mater. Chem. C* **2017**, *5*, 6547.
[9] G. Cai, S. Park, X. Cheng, A. L.-S. Eh, P. S. Lee, *Sci. Technol. Adv. Mater.* **2018**, *19*, 759.
[10] T. S. Hernandez, M. Alshurafa, M. T. Strand, A. L. Yeang, M. G. Danner, C. J. Barile, M. D. McGehee, *Joule* **2020**, *4*, 1501.
[11] Y. Rao, J. Dai, C. Sui, Y.-T. Lai, Z. Li, H. Fang, X. Li, W. Li, P.-C. Hsu, *ACS Energy Lett.* **2021**, *6*, 3906.
[12] K. Dong, D. Tseng, J. Li, S. Warkander, J. Yao, J. Wu, *Cell Rep. Physical Sci.* **2022**, *3*, 101066.

[13] J. Niu, Y. Wang, X. Zou, Y. Tan, C. Jia, X. Weng, L. Deng, *Appl. Mater. Today* **2021**, *24*, 101073.
[14] J. G. Metts, J. A. Nabity, D. M. Klaus, *Adv. Space Res.* **2011**, *47*, 1256.
[15] P. Chandrasekhar, B. Zay, T. McQueeney, A. Scara, D. Ross, G. Birur, S. Haapanen, L. Kauder, T. Swanson, D. Douglas, *Synth. Met.* **2003**, *135*, 23.
[16] a) P. Chandrasekhar, B. J. Zay, D. Lawrence, E. Caldwell, R. Sheth, R. Stephan, J. Cornwell, *J. Appl. Polym. Sci.* **2014**, *131*, 39900; b) N. Kislov, H. Groger, R. Ponnappan, *AIP Conf. Procee.* **2003**, *172*, 654; c) H. Demiryont, K. C. ShannonIII, *AIP Conf. Proc.* **2007**, *880*, 51; d) X. Wang, H. Jin, B. Wang, C. Ling, J. Yang, D. Li, J. Li, *J. Appl. Phys.* **2022**, *131*, 125102; e) R. B. Mulford, S. D. Salt, L. P. Hyatt, K. S. Meaker, V. H. Dwivedi, M. R. Jones, B. D. Iverson, *Appl. Therm. Eng.* **2020**, *178*, 115658; f) S. Taylor, N. Boman, J. Chao, L. Wang, *Appl. Therm. Eng.* **2021**, *199*, 117561.
[17] C. Sui, J. Pu, T.-H. Chen, J. Liang, Y.-T. Lai, Y. Rao, R. Wu, Y. Han, K. Wang, X. Li, *Nat. Sustain.* **2023**, *6*, 428.
[18] A. Ghanekar, J. Wang, S. Fan, M. L. Povinelli, *ACS Photonics* **2022**, *9*, 1157.
[19] M. Babucci, V. Balci, A. Akçay, A. Uzun, *J. Phys. Chem. C* **2016**, *120*, 20089.
[20] D. Yongquan, W. Ming, C. Lin, L. Mingjun, *Desalination* **2012**, *295*, 53.
[21] R. Liang, M.-R. YANG, Q.-X. ZHOU, *Acta. Phys. Chim. Sin.* **2010**, *26*, 1468.
[22] Y. NuLi, J. Yang, R. Wu, *Electrochem. Commun.* **2005**, *7*, 1105.
[23] a) K.-S. Kim, B.-K. Shin, H. Lee, *Korean J. Chem. Eng.* **2004**, *21*, 1010; b) R. Bomparola, S. Caporali, A. Lavacchi, U. Bardi, *Surf. Coat. Technol.* **2007**, *201*, 9485.
[24] Y. Huo, S. Xia, S. Yi, P. Ma, *Fluid Phase Equilib.* **2009**, *276*, 46.
[25] a) K. Huang, Y. Wang, H. Mi, D. Ma, B. Yong, P. Zhang, *J. Mater. Chem. A* **2020**, *8*, 20593; b) J. Jaganathan, M. Sivapragasam, C. Wilfred, *J. Chem. Eng. Process Technol.* **2016**, *7*, 1.
[26] F. Shaahmadi, B. H. Shahraki, A. Farhadi, *J. Chemical Thermody.* **2020**, *141*, 105922.
[27] J. Mohammed-Ibrahim, X. Sun, *J. Energy Chem.* **2019**, *34*, 111.
[28] F. Liu, Y. Deng, X. Han, W. Hu, C. Zhong, *J. Alloys Compd.* **2016**, *654*, 163.
[29] R. Fukui, Y. Katayama, T. Miura, *J. Electrochem. Soc.* **2011**, *158*, D567.
[30] N. Kanani, *Electroplating: Basic Principles, Processes and Practice*, Elsevier, Amsterdam **2004**.
[31] O. Kasian, N. Kulyk, A. Mingers, A. R. Zeradjanin, K. J. Mayrhofer, S. Cherevko, *Electrochim. Acta* **2016**, *222*, 1056.
[32] X. Hou, Z. Wang, J. Pan, F. Yan, *ACS Appl. Mater. Interfaces* **2021**, *13*, 37339.
[33] A. Dębski, S. Terlicka, A. Budziak, W. Gąsior, *J. Alloys Compd.* **2018**, *732*, 210.
[34] I. Lopez-Salido, D. C. Lim, Y. D. Kim, *Surf. Sci.* **2005**, *588*, 6.
[35] Q. Shu, J. Demko, J. Fesmire, *IOP Conf. Ser. Mater. Sci. Eng.* **2017**, *278*, 012133.
[36] a) H. Demiryont, D. Moorehead, *Sol. Energy Mater. Sol. Cells* **2009**, *93*, 2075; b) E. N. Taylor, L. M. Diele-Viegas, E. J. Gangloff, J. M. Hall, B. Halpern, M. D. Massey, D. Rödder, N. Rollinson, S. Spears, B. j. Sun, *J. Exp. Zoology Part A: Ecological Integrative Physio.* **2021**, *335*, 13.
[37] Z. Ma, Q. Wang, Z. Wu, D. Chen, C. Yan, Y. Shi, M. D. Dickey, B. Su, *Adv. Mater.* **2022**, *34*, 2203814.
[38] T. D. Swanson, G. C. Birur, *Appl. Therm. Eng.* **2003**, *23*, 1055.
[39] V. P. Patel, R. Barido, B. Johnson, T. Ibarra, *SAE Tech. Pap.* **2001**.
[40] F. Incropera, D. DeWitt, *Fundamentals of Heat and Mass Transfer*, Ed.: 3rd, Wiley, New York, **1985**.